LANGMUIR

pubs.acs.org/Langmuir Article

Three-Dimensional Sag Tracking in Falling Liquid Films

Marola W. Issa,*[,11] Hairou Yu,[11] Maria Chiara Roffin, Steven V. Barancyk, Reza M. Rock, James F. Gilchrist, and Christopher L. Wirth

Cite This: Langmuir 2022, 38, 11581−11589 Read Online

ACCESS | Metrics & More Article Recommendations Supporting Information

ABSTRACT: Coating defects often arise during application in the flash stage, which constitutes the ~10 min interval immediately following film application when the solvent evaporates. Understanding the transient rheology and kinematics of a coating system is necessary to avoid defects such as sag, which results in undesirable appearance. A new technique named variable angle inspection microscopy (VAIM) aimed at measuring these phenomena was developed and is summarized herein. The essence of this new, non-invasive, rheological technique is the measurement of a flow field in response to a known gravitational stress. VAIM was used to measure the flow profile through a volume of a liquid thin film at an arbitrary orientation. Flow kinematics of the falling thin film was inferred from particle tracking measurements. Initial benchmarking measurements in the absence of drying tracked the velocity of silica probe particles in ~140 μm thick films of known viscosity, much greater than water, at incline angles of 5° and 10°. Probe particles were tracked through the entire thickness of the film and at speeds as high as ~100 μm/s. The sag flow field was well resolved in 10 μm thick cross sections, and in general the VAIM measurements were highly reproducible. Complementary profilometer measurements of film thinning were utilized to predict sag velocities with a known model. The model predictions showed good agreement with measurements, which validated the effectiveness of this new method in relating material properties and flow kinematics.

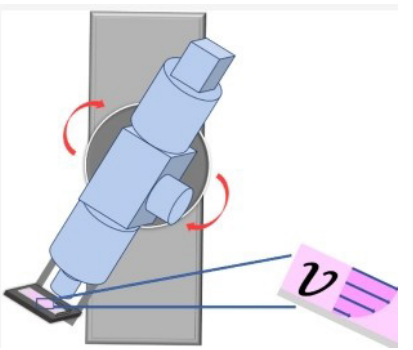

1. INTRODUCTION

Along with protecting the substrate and coating layers below, one of the primary functions of decorative coatings such as automotive topcoat systems is to present a smooth, "mirror-like" finish. Controlling this finished appearance is of crucial importance, particularly in the automotive industry. Parameters such as the coating composition, substrate geometry, film thickness, and other processing factors work interdependently to produce the final appearance.[1] Inadequate control of coatings during the process and application stages can lead to multiple defects including cratering, orange peel, dripmark formation, and sag.2 These defects arise from the complex interplay of transient rheology and fluid flow that occurs when solvent evaporates from a coating during flash. Flash refers to the stage during which the solvent evaporates at ambient conditions. Subsequent steps, such as thermal or UV curing, will arrest these structural deficiencies, potentially resulting in permanent functional defects and aesthetically unappealing features. As to the global interest and market impact of this work, according to the Automotive Coatings market report by BCC Research (report code CHM075D), in 2021, global automotive clear coat sales totaled $2.09 billion, out of the total automotive coating market of $10.29 billion. Furthermore, note that such challenges are not unique to the paint industry. Defects that arise during solvent evaporation are also relevant for food and pharmaceutical coatings.3

"Sag", which results from a coating responding to a gravitational stress, is one undesirable phenomenon that may occur during flash. Sag causes a host of undesirable features, mainly leading to accumulation of material in unintended regions. This causes an increase in edge thickness down the slope due to sample accumulation over the coating substrate.[4] Sag may occur when the viscosity of the coating does not increase quickly enough to inhibit the flow immediately after application.[5] Additionally, the viscosity of coatings may also vary throughout different depths, relative to the free surface, due to gradients in the solvent concentration as it diffuses through the film and evaporates.[6] The reduction in the solvent content with time can result in microstructure formation (i.e., polymer entanglement), leading to sufficient coating elasticity,[7] allowing the material to resist changes in its volume or shape under mechanical stresses such as gravity.[8] Furthermore, the elastic response of a material is related to its yield stress, which can affect the flow properties and formation of sag.[9] Considering the energy-intensive nature of the application stage for automotive coatings, the need for accurate inspection

Received: May 16, 2022
Revised: August 30, 2022
Published: September 12, 2022

https://doi.org/10.1021/acs.langmuir.2c01232
Langmuir 2022, 38, 11581-11589

to enable a priori prediction of the coating performance is crucial.[10] Over the last few decades, a variety of optical and non-optical techniques, including the "indicator" method, falling wave technique, and distinctness of ima e (DOI) apparatus, were developed to help evaluate sag.[5,11] - [4] Despite the individual merits of these techniques and their robustness, the need for a method that enables real-time quantitative evaluation of sag is necessary.

The classical problem of a falling liquid film was previously investigated, with many efforts focusing on models developed to further understand the relevant phenomenon.[15-21] One early contribution focused on a viscous liquid film that was positioned at an incline. This problem was treated with a lubrication approximation to yield a similarity solution that effectively predicted the shape of a film as it traveled down an inclined plane.[20] Another excellent recent contribution used lubrication theory to predict the shape of a drop of suspension as it responded to gravity.[22] One key assumption in this model was that of "rapid-vertical-diffusion", or when transport in the z-direction is sufficiently fast such that only gradients in the *x*-direction are considered. Furthermore, this modeling effort assumed a perfectly wetting droplet with a known suspension rheology. The framework provides a platform for exploring several effects (i.e., wetting) and will be further explored in future work. Other efforts in this area include predicting how thin films flow over heated surfaces and elucidating the impact of surface topography.[23,24] Additionally, the effects of capillary buildup at the film edge were further studied to demonstrate the dynamics of film wetting and spreading.[25,26]

Evaluating sag in industry commonly relies on a visual technique certified by the American Society of Testing and Materials (ASTM D4400). This technique uses a U-shaped drawdown bar called an anti-sag meter, which has multiple notches of identical width and varying clearances. Upon coating application, a series of wet parallel stripes of identical widths and varying thicknesses are generated. The substrate housing the films is oriented at 90°, where the stripes are parallel to the ground with the thickest stripe at the bottom. Anti-sag properties of material are correlated to an index value which corresponds to the smallest thickness in which no two stripes are seen to completely merge.[27] This testing method provides some advantages in that it is simple and robust. However, little quantitative information can be learned about the flow fields inherent to the sag process. ASTM D4400 is conducted at 90° and has neither spatial nor temporal resolution through films, thereby preventing the study of flow instabilities (e.g., Marangoni-Benard convection) with this technique. In addition to ASTM D4400 standard, there are other variations to explore the phenomena of sag. Herein, we summarize the development of a complementary technique that seeks to provide a fundamental understanding of the complex relationship between rheology and kinematics in the phenomena that leads to sag.

We developed a variable angle inspection microscope (VAIM) to measure the sag velocity through the depth of a liquid thin film. The VAIM uses a piew-controlled objective that helps to capture a series of images at variable heights throughout the film, facilitating the tracking of probe particles at various depths. This new technique enables for accurate measurements of the velocity profile throughout the entire depth of the film as opposed to the flow velocity at the free surface. The thickness-resolved sag profile provides an advantage over existing technologies and allows for probing a wide range of substrate geometries and fluid compositions. Furthermore, it enables the investigation of the effects of substrate properties (i.e., roughness) very near the substrate itself. Of note is the flexibility afforded by the VAIM to vary the substrate angle. The coating (or generally any sample) can be probed via systematic variation of this angle with respect to gravity. This flexibility in rotation allows dynamic analysis of the flow field, where the angle of incline can be continuously changed. The results summarized herein focus on benchmarking this technique using non-flashing liquids of constant viscosity. The repeatability and robustness of the method will allow direct measurement of the velocities and, more generally, the kinematics, of a coating undergoing solvent evaporation in the future.

2. THEORY

2.1. Thin Liquid Film Flow down an Incline. Thin liquid films, when positioned at an incline angle *0* with respect to a horizontal plane, experience a combination of gravitational and viscous forces. Briefly, the gravitational force Fg drives flow down the incline (eq **1**) and the viscous force *F.* opposes flow (eq 2). For the case of one-dimensional flows

$$= WL\ \rho g\ \sin(0)x(t) \quad \textbf{(1)}$$

$$F_v = \frac{WL}{\mu}\frac{dv}{dx} \quad (2)$$

where W is the film width, L is the film length, g is the acceleration due to gravity, ρ is the film density, v is the local velocity,μ is the sample viscosity, and $x(t)$ is the plane depth relative to the initial free surface (see Figure 1). Those two

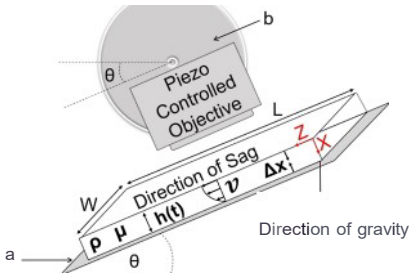

Figure l. VAIM and particle tracking setup. (a) Microscope slide used as a substrate for film application and (b) goniometer which allows the setup to rotate to any desired angle *0*.

forces are balanced at the steady state. The effects of surface tension are neglected in the present analysis but could play a role in our experimental results as described later in the article. However, in cases of unsteady flows away from equilibrium, there could be an imbalance in viscous, gravitational, and surface tension forces, leading to fluid flow instabilities.[28] Moreover, the inclusion of an evaporating solvent as is the case for coatings will complicate the flow field. Herein, we focus on the simplest case in which the forces are in balance and the Newtonian liquid solvent does not evaporate to illustrate the experimental technique.

In general, the rheology of the film governs the sag velocity profile through the depth of the coating.[29] The thin films utilized in this study consist of non-evaporating petroleum-based mineral oils with known constant viscosities. Thus, the one-dimensional flow is solely influenced by the balance of

https://doi.org/10.1021/acs.langmuir.2c01232
Langmuir 2022, 38, 11581-11589

gravitational and viscous forces and is only limited by the volume of material deposited onto the substrate. Consequently, assuming no slip at the substrate surface, the velocity of a falling film is represented by (eq 3).

$$v = \int \frac{\rho g x(t) \sin(\theta)}{\mu}\, dx \tag{3}$$

With the assumptions of steady state and incompressible one-dimensional flow down an incline, the velocity of a fallin§ Newtonian film with constant viscosity has been derived.3 This form is obtained from the abovementioned general expression and is given by (eq 4). Note that herein we allow both the position at which the velocity is evaluated $x(t)$ and the film thickness $h(t)$ to vary in time to match the way in which experiments are conducted. The laboratory temperature during video capture was utilized for calculating the viscosity and density of each sample from the tabulated data.

$$\mu = \frac{\rho g [h(t)^2 - x(t)^2] \sin(\theta)}{2\mu} \tag{4}$$

2.2. Expression for the Thinning of a Liquid Film. A thin film of liquid flowing down an inclined plane is a well-studied physical phenomenon regularly encountered throughout industry.[31-3] There are well-established models based on lubrication theory for the time and space evolution of thickness of a film responding to gravity.[20,22] One such model predicts the time and space evolution of film thickness, $h(t) = ((11/g)\sin(\theta))^{1/2}(z/t)^{1/2}$ at some angle of inclination, θ, with a fluid of kinematic viscosity, μ, responding to gravity, g, in time, t.[20] Herein, we tested this model to evaluate the efficacy of predicting our experimental measurements to furnish thickness values that would then be used to predict velocity via eq 4. Although the model yields excellent predictions of the shape of the film thinning dynamics at longer times ($t > 2$ min), it did a poor job at short times ($t < 2$ min) (see Figure SS in the Supporting Information). We chose instead to use a semi-empirical model that enabled the prediction of accurate height measurements for all times.

Considering the limited material volume deposited for each sample, the film thickness h is expected to decrease over time as the film sags downward. Our semi-empirical approach for approximating film thickness was to assume a constant volume and constant width deformation of the liquid film with a pinned trailing-edge, such that only the leading-edge position and film thickness changed as a function of time. For a volume of film V with width W, length L, and height h, the change in film thickness $h(t)$ is predicted from the change in volume over time which remains constant (eq 5).

$$\frac{dV}{dt} = \frac{d(W L h)}{dt} = 0 \tag{5}$$

Assuming W is constant, the abovementioned equation is rewritten as partial derivatives in terms of L and h and rearranged to provide a mathematical expression for the change in thickness over time dh/dt, as shown in (eq 6)

$$\frac{dh}{dt} = \frac{h}{L}\frac{dL}{dt} \tag{6}$$

Sag denotes the change in film length over time dL/dt. This phenomenon is attributed to effects of gravity, which is computed from the average sag velocity, in addition to a fitting parameter Gamma Γ, obtained from the profilometry measurements (eq 7). Gamma accounts for the added velocity component not captured by the average velocity. We expect this variable relates to the increase in velocity consistent with material accumulation downstream, which further increases the gravitational forces acting on the film.

$$\frac{dL}{dt} = (\text{II}) + \Gamma = \frac{\rho g \sin(\theta) h^2}{6\mu} + \Gamma \tag{7}$$

Substituting eq 6 into 7, the change in height over time yields the following expression (eq 8)

$$\frac{dh}{dt} = -A h^4 - Bh^2 \tag{8}$$

where A and B are constants and are equal to $\frac{\rho g \sin(\theta)}{3\mu}$ and $\frac{\Gamma}{V}$, respectively. Solving the abovementioned mathematical expression by integration and assuming appropriate boundary conditions, such that at time $t = 0$, the film thickness is the initial thickness measured from profilometry h_0 and for $t > 0$, the film thickness $h_0 > h(t) > 0$ yields (eq 9).

$$\frac{A^{0.5}\,\mathrm{ArcTan}\left(\frac{h_0}{B^{0.5}}\right)}{B^{0.5}} - \frac{1}{Bh(t)} = A^{0.5} h_0 \mathrm{ArcTan}\left(A^{0.5} h_0\right) + \frac{1}{2}\ln\left(1 + A h_0^2\right) \tag{9}$$

Equation 9 was used to predict the film thickness for experiments, but additional understanding was obtained via solution of eq 8 after malting it dimensionless. Rescaling the independent and dependent variables by using $h = \frac{h(t)}{h_0}$ and $t = \frac{t}{t_0}$, the film thinning expression in eq 9 takes on the non-dimensional form shown below in (eq 10).

$$\frac{dh}{dt} = -\frac{\mu}{6\rho r h_0} Ga h^4 - h^2 \tag{10}$$

where Ga represents the Galileo number which balances the gravitational forces and viscous forces acting on the film, such that $Ga = \frac{\rho g \sin(\theta) h_0^3}{\mu^2}$, h is the initial thickness of the film, and t_0 is equal to the quotient of L and Γ, $t_0 = L/\Gamma$, with dimensions of time. Further collection of variables leads to the following expression

$$\frac{dh}{dt} = -\Gamma h^4 - h^2 \tag{11}$$

where $\Gamma = \frac{\rho g \sin(\theta) h_0^3}{6\Gamma\mu}$ and with the boundary condition $h(t = 0) = 1$. Equation 11 has the following solution

$$t = \Gamma'[\tan^{-1}(h(t)f) - \tan^{-1}(f')] + \frac{j}{h(t)} - 1 \tag{12}$$

3. EXPERIMENTAL SECTION

3.1. Materials. Fluorescently labeled (~1 μm) silica particles were synthesized via the Stober method.[34] This technique utilized a silica precursor, tetraethyl orthosilicate (TEOS), which in the presence of ethanol (200 Proof, 99.5% purity) and ammonium hydroxide (NH_2OH) undergoes hydrolysis, followed by a polycondensation

https://doi.org/10.1021/acs.langmuir.2c01232
Langmuir 2022, 38, 11581-11589

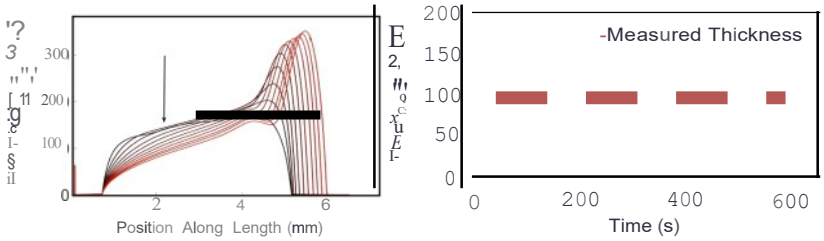

Figure 2. Surface topography scans for S200 samples at 10° incline. *As* the coating sags, accumulation of film down the incline increases. This is seen in the progression of peaks, which has an initial value of~ 160 μm and a final value of ~350 μm. The initial scan at time t = 0 is represented by the black line, and the consecutive scans collected at 1 min interval progress to bright red at t = 10 min. The *x-axis,* position along the length (mm), depicts the direction of both sagand profilometer scans, where x = 0 represents the initial analyzed point with the scan direction in the positive x-direction. The arrow points to the region in which particle tracking was conducted for all samples. This region represents one-third of the distance from the coating upstream. The height decay data in the ROI show an initial thickness of ~150 $\mu m$and a final thickness of ~85 µmas seen on the right panel.

reaction to produce non-porous silica particles. Rhodamine-B Isocyanate (RBTC) was incorporated in the synthesis process to make the particles fluorescent. The particles were then added to the samples, and the mixtures were sonicated to ensure homogeneous distribution of particles in solution. Rinsed and dried probe particles were incorporated at ~0.09% volume fraction in all samples (see Figure Sl in the Supporting Information for SEM images).

Three petroleum-based viscosity standards with known densities and dynamic viscosities were utilized: N35 (ρ = 0.8567 g/mL, μ = 74.13 mPa s), S60 (ρ = 0.8609 g/mL, μ = 135.1 mPa s), and S200 (ρ = 0.8567 g/mL, μ = 568.4 rnPa s) at 20 °C. The general standards were purchased from Sigma-Aldrich; Lot #2192207052, Lot #7190511023, and Lot #1192409082, respectively. See Figure S6 in the Supporting Information for a summary of material properties. The laboratory temperature was taken into consideration for each experiment for accurate approximation of the film viscosity and density.

3.2. Film Preparation and Measurement Methods. The application process utilized an automatic drawdown machine (Byko-Drive G. 2122) and a 3 in. casting knife obtained from BYK instruments. The setup also included a custom-made drawdown plate, which can accommodate a 25 X 75 mm microscope slide. The orientation of the drawdown machine was controlled such that the angle of drawdown was 0°. For each experimental run, 80 μL of sample volume was pipetted onto the microscope slide and the casting knife was set to motion at 25 mm/s with 10 mils (254μm) drawdown film thickness. Note that the actual film thickness is typically around half the value of the drawdown thickness. The film thickness analyzed is ~150 μm, as seen in the Results and Discussion section. The samples were immediately transferred to the VAIM for particle tracking.

Figure 1 shown below is a schematic of the VAIM and particle tracking apparatus. The components of VAIM are a CMOS digital camera (Thorlabs DCC1240C-HQ), tube lens for the objective, an objective (Olympus UPLFLN20X), a goniometer, a light source, and fluorescence filters (Thorlabs TXRED MF559-34) to facilitate the epifluorescence measurements. The filter piece accommodates an input white light source, emission and excitation filters, and dichroic filters. A Texas Red filter set was utilized, with an emission filter (630 ± 34.5 nm), an excitation filter (559 ± 17 nm), and a dichroic filter (reflection: 533-580 nm, transmission: 595-800 nm). Additionally, the setup includes a custom 3D-printed piece as a sample holder. VAIM operates like a regular microscope, with the main difference being that the sample can be observed at any orientation with respect to gravity while keeping the direction of observation normal to the substrate. This allows for the horizontal focal plane to remain parallel to the substrate for all various orientations relative to gravity.

3.3. Video Capture, Image Processing, and Particle Tracking Method. Raw videos had dimensions of 1280 X 1024 pixels and were RGB color images. Raw data were first converted to an 8-bit format and cropped to include most captured particles. The average dimension of all ROI analyzed was 989 X 802 pixels. Video capture was done immediately following film application via an automatic drawdown machine. The duration of videos was ~ 10 min. Prior to video capture, the piezo controller was programmed by utilizing the height thinning data obtained from profilometry, in conjunction with a calibration slide which was used to locate the solid- liquid interface. Thinning was tracked via surface topography with a NANOVEA ST400 profilometer. The surface analyzer utilized has a lateral resolution of2.6 μm,a 1.1 mm depth-range, and a height repeatability of 23 nm within that range. The optical profilometer utilized allowed for conducting non-contact scans of the flowing liquid films. Thus, liquid flow was not disrupted.[35] Moreover, horizontal scans were conducted continuously, at a rate of one scan per minute, for 10 min with an average of ~ 25 s per scan. This allowed for monitoring the thinning process by measuring changes in sample thickness over time. Although the dynamic boundary was different for the various viscosity standards, the scanning process followed the same step motion of 10 μm and delay time of 5 s. All videos were collected at a rate of 10 frames per second (FPS) with an exposure time of ~ 100 ms. Each experimental video was analyzed with a standard particle tracking algorithm executed in MATLAB for sag velocity measurements.[36]

4. RESULTS AND DISCUSSION

4.1. Thinning of a Sagging Film. Initial work focused on measuring the thinning process of a liquid film as it sagged down an incline. This information was required to then make predictions of the sag velocity (via eq 4) at different positions within the film. Furthermore, knowledge of the thinning process was helpful for designing the volume scans for each viscosity standard at the desired incline. Figure 2 shows representative data of a full profilometer scan from the S200 sample at a 10° incline. Note that particle tracking for velocity measurements was conducted at one-third the distance from the coating upstream for all samples (as shown by the black arrow in Figure 2). This position was chosen to avoid the region of the film downstream that experienced material accumulation.

Data from the profilometer scans were then incorporated into the falling film model for prediction of particle sag velocity. A semi-empirical model (eq 9) was used to incorporate these data into the velocity prediction [$h(t)$ in eq 4]. Film thickness as a function of time is shown for N35 at a 5° incline in Figure 3. Solid red dots represent the measured film thickness at discrete time points, while the solid black line is the Gamma fit as described by eq 9. The fit worked well for the purposes of representing the discrete data, in that the typical error associated with the height prediction was <5%. Given that the fit closely followed the experimental measure-

https://doi.org/10.1021/acs.langmuir.2c01232
Langmuir 2022, 38, 11581-11589

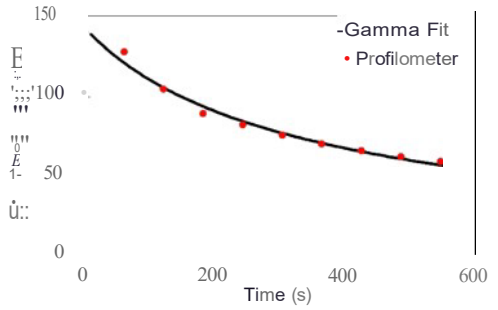

Figure 3. Height decay fitting curve for N35 at 5° incline. The red dots are the measured film thickness obtained from surface analyzer measurements. The solid black line is obtained from the gamma fit shown in eq 9. The initial film thickness for this sample is ~145 μm and the final thickness is ~55 μm.

ments, we utilized this expression as input parameters for the velocity prediction model.

Finally, film thinning was interpreted via the dimensionless model given by eq 12. The dimensionless expression depends on the parameter f, which is the square root of the ratio of the initial average sag velocity and anomalous velocity contribution. The average value off across all experimental conditions was f $= 0.65 \pm 0.18$. This value was then used to calculate the dimensionless thinning profile and compared with all data (see Figure 4). Note that the error reported with f is the standard

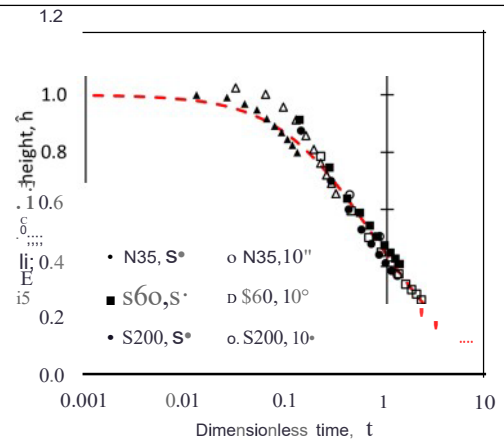

Figure 4. Dimensionless thinning profile for all experimental conditions as compared to the average master curve (broken red line). Data shown in this figure demonstrate the universality of the process and the consistency of the anomalous velocity contribution, suggesting systematic and physical origins of r across all experiments. We will test for the origin of r in future experiments with systematic variation in substrate wettability.

deviation of the average as obtained from values off foreach experiment. Experimental data collapsing onto the master curve demonstrate the universality of the thinning process, even in the presence of an anomalous contribution to velocity inr.

Although the fundamental dependence of r on various materials is not yet known, there are observations from experiments that may help identify the origin of non-zero r. The most likely cause is in the non-uniform wetting of the downstream substrate as the film sags. Data summarized in Figure 2 show material accumulation downstream, where the local curvature is small, ca ~ 1, and the dynamics are influenced by surface energy. The film thinning expression scales to Galileo number and the fitting parameter Gamma. Gamma was observed to display a linear trend with the Galileo number, such that both parameters increase with increased angle of incline and/or decreased viscosity (~dh/dt large). *As* the film thinning takes place upstream, material accumulates down the incline. Mass accumulation, as seen in the propagation of peaks in profilometry measurements, leads to an increase in the local film thickness downstream. This region also exhibits a relatively smaller width, thus classifying the sag in this case as nonuniform sag (i.e., dripping). This causes an increase in the gravitational forces acting on the film downstream and higher velocity measurements, which depends on the square of the film thickness, as opposed to predicted values. Such additional contributions to the velocity are the most likely origin of r.

4.2. Thickness Resolved Velocity Profile in a Falling Film. The velocity distribution throughout the depth of films was measured with three repeats per condition, which consisted of the three fluids described above and two different inclines for a total of 18 experiments. Particle tracking was conducted at one-third of the coating upstream, as per the guidance of Section 4.1 Figure 2. Representative data, consisting of the N35 sample at a 5° incline angle, for these experiments are shown in Figure 5. Note those data on the

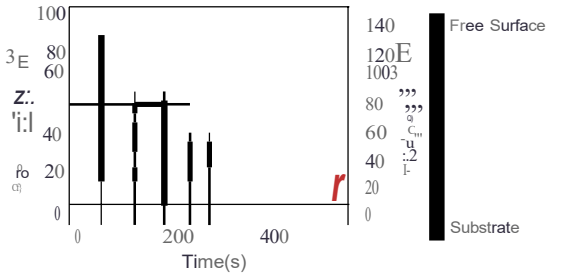

Figure 5. Measured particle velocity (μm/s) over time (sec) for N35 at 5° incline. The highest velocity was measured at the free surface, data from which are shown by the bright red circles. The velocity decreased deep into the film and reached zero at the substrate; these data are shown by the black circles. Each peak represents one scan cycle in and out of the film starting at the free surface and then returning to the free surface. The peaks progressively decreased in size indicating a decrease in particle velocities as the film thickness decays. The black line is the thickness of the film, whereas the slope of that line represents the rate of thickness decay *(μm/s)* measured with the surface analyzer at 5° incline. Error bars represent the standard deviation associated with the measured velocity obtained via the particle tracking algorithm.

primary *y-axis* contain information about not only sag velocity but also the depth in the film. The color of individual points, namely, the intensity of red, indicates depth relative to the free surface. Those data from near the free surface are red, whereas data collected near the substrate are black. The secondary *y*-axis shows the film thickness as measured with a profilometer. Both data sets are plotted as a function of time.

Sag velocity as measured with the VAIM has a saw-tooth pattern because of the scanning path taken by the objective (see Figure 5). The piezo adjusted the vertical position of the objective, scanning the ROI from roughly the free surface to the substrate. Sag velocity was measured to be at its largest value near the free surface and decayed to zero near the boundary. Additionally, the mean velocity decayed over time as the finite volume coating decreased in thickness. This behavior

https://doi.org/10.1021/acs.langmuir.2c01232
Langmuir 2022, 38, 11581-11589

was expected because the fluid velocity is directly proportional to the square of film thickness at the fixed observation plane *x(t)* (see eq 4). These trends were observed in all samples at both 5 and 10° incline angles.

Beyond the physical phenomena revealed via measurement of the fluid flow, there are several important features of these data suggesting that V**AIM** is well suited for application with industrially relevant coating systems. First, the V**AIM** was able to track particles through the entire depth of a thick liquid film. Typical automotive coatings applications are <10 mils, which is thinner than those used herein. One would expect imaging conditions to improve for thinner films, especially those that have similar optical properties to these model systems, such as clear coats. This suggests that the use of the VAIM for industrially relevant systems is feasible with respect to film thickness. Moreover, the sag flow field was sufficiently slow such that regular speed imaging **(10** fps) was suitable to capture particle translation even for the least viscous fluid, N35. Although capturing flow fields with a larger velocity would be feasible with a high-speed camera (as will be described later in the article), these data show that a typical sag flow field can be captured with an economical camera option suitable for manufacturing or quality control laboratory environments. Moreover, a sufficiently slow flow field facilitates particle tracking without merging and mixing of streamlines that could occur at much larger flow rates.

Finally, experiments were also repeatable. Figure 6 shows three experimental repeats for the N35 sample at a 5° incline.

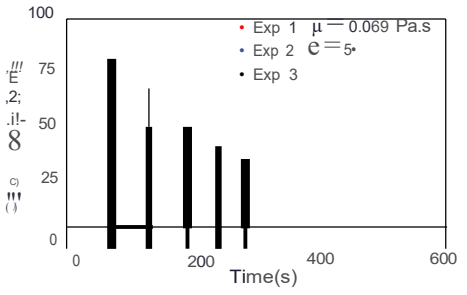

Figure 6. Three experimental repeats for N35 at 5° incline. The experiments were highly reproducible at various conditions, that is, viscosities and incline angles. This validates the robustness and repeatability of VAIM. Error bars represent the standard deviation of measured velocity.

The measured particle velocities for all conditions were highly reproducible which validates the efficacy ofVAIM in probing a three-dimensional volume of fluid. The error bars represent the standard deviation of the measured velocity as obtained from the particle tracking algorithm. Run-to-run variation in standard error can be explained by the nature of the experimental setup. Video capture was initiated immediately following reorientation of the film at an incline. However, each run had slightly varying moments in times during which the planes were filmed.

Experiments were conducted with fluids of systematically varied viscosity. Figure 7 compares the sag velocity for N35, S60, and S200 at 5 and 10° incline angles. The qualitative shape of all velocity distributions was the same as those shown earlier, with a saw-tooth pattern and a mean velocity that decayed as the film thinned. Both sets of data, for 5 and 10° incline angles, show the N35 and S60 samples to have similar velocity distributions. These data also show that an increase in viscosity at fixed orientation leads to a smaller velocity decay in time, as seen from comparing results from N35 (0.069 Pa s) and S200 (0.504 Pa s). Although the thin film of N35 experienced a steep decay in sag velocity, the sag velocity for S200 was relatively flat at both orientations. These data are consistent with the film thinning measurements in which the N35 had a change in height of ~92 and ~ **111** *μm* and S200 had a change in height of ~32 and ~64 *μm* at 5 and 10°, respectively. The more viscous film, which thinned to a lesser extent as compared to N35, experienced a velocity distribution with a less substantial decay in mean velocity. Finally, as shown in both Figures 7 and 8, the velocity distribution had the same

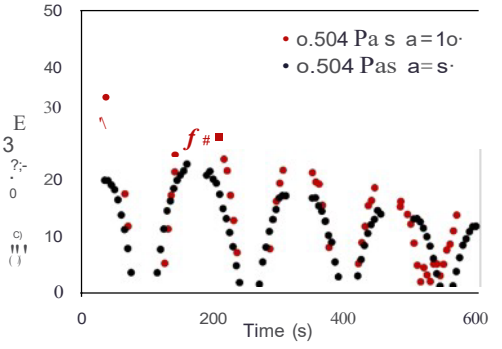

Figure 8. Measured sag velocity for S200 at 5 and 10° incline angles. The slight increase in the angle of incline led to an increase in the measured velocity because of the increased gravitational force acting on the film.

qualitative shape, but the magnitude depended on the inclination angle. For instance, the S200 (0.504 Pas) viscosity standard at both 5 and 10° incline angles. The velocity

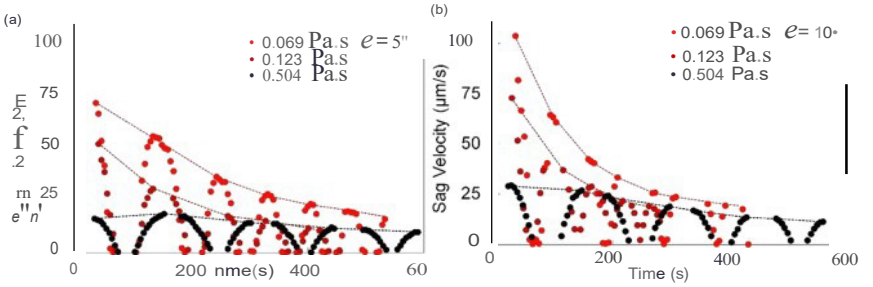

Figure 7. Sag velocity for N35, S60, and S200 at 5° incline angle (a) and 10° incline angle (b). The velocity distribution follows a similar trend for various viscosities. The sag velocity is at a maximum velocity value at the free surface and decreases deep into the film. An increase in viscosity at fixed orientation led to a smaller velocity decay in time, as seen from comparing results from N35 (0.069 Pas) andS200 (0.504 Pas).

https://doi.org/10.1021/acs.langmuir.2c01232
Langmuir 2022, 38, 11581-11589

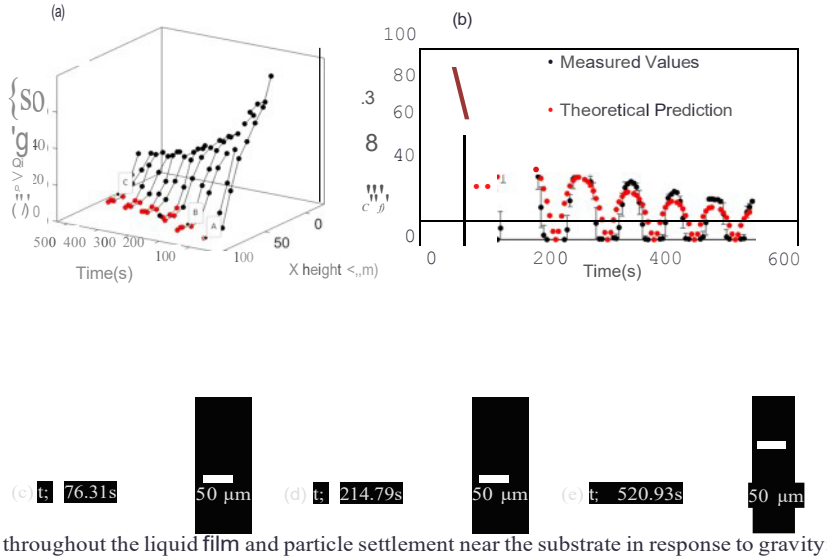

Figure 9. Sagvelocity profile throughout the liquid film and particle settlement near the substrate in response to gravity: (a) The velocity profile for N35 at 5° incline angle. The *x-axis* is the height which indicates the depth from the free surface. A higher *x* value means the plane was near the solid interface, and the smaller value corresponds to the plane near the free surface. The red dots represent the velocity at 2 *µmis,* which reaches a plateau for planes near interfacial regions. (b) Measured velocity (black dots) and the theoretical (red dots) velocities (µm/s) for N35 at 5° incline. The model predictions show excellent agreement with measurements obtained by the overlap in data, and the plateau near the substrate and near the free surface show disagreement of the velocity. (c-e) Settlement and accumulation of fluorescent particles (red) at three times which are selected as A, B, and C in (a) near the substrate. The increase in particle visibility as seen from the red pixels displayed suggests particle settlement in response to gravity. The sedimentation velocity was noted to be orders of magnitude smaller than the transverse velocity in film.

measurements are larger at the higher inclination angle due to the higher imposed stress.

4.3. Measurements as Compared to Predictions. Measurements conducted with the VAIM were compared with predictions furnished by eq 4. Input values for the model included the physicochemical properties of the fluid density *p* and viscosity *µ* (adjusted for laboratory temperature), inclination angle *0,* observation plane position *x(t),* and film thickness *h(t).* Although all other parameters are known as a material property or experimental condition, film thickness as a function of time was measured and subsequently utilized by the Gamma fit function from measurements conducted with a profilometer. As noted above, a profilometer provides thickness measurements at discrete points in time. However, a continuous function for *h(t)* was used to facilitate model predictions by fitting the discrete time points with the expression as described in an earlier section.

Figure 9a is a three-dimensional plot displaying the velocity profile for N35 at a 5-degree incline. The measured velocity in the region close to the solid boundary is underpredicted. This can be seen as the measured data reach a plateau near layer 200, which represents the solid-liquid interface. For the least viscous samples at smaller incline angles, the measured velocity near the substrate is underpredicted due to particle settling which is more prominent in samples with smaller viscosity. The particles which settle down are tracked through multiple layers near the boundary due to their small threshold value, which makes excluding them in the tracking algorithm not possible. Similarly, a plateau is observed in the layers close to the free surface for the same low viscosity samples. This is due to particles being tracked at multiple different layers, which affects the overall average velocity measured in each plane.

Figure 9b shows a comparison between measured and theoretical velocities (µm/s) for N35 at a 5° incline. The black dots represent the measured velocities obtained from particle tracking, and the red dots are the theoretical velocities. These data show excellent qualitative agreement between the model predictions and measurements. As was the case with experimental measurements, the predicted sag velocity had a saw-tooth pattern in which the maximum velocity occurred near the free surface and the minimum (~0 *µm/s)* occurred near the boundary. Furthermore, the mean velocity decays over time because of film thinning. These data further validate the effectiveness of this method in measuring the local flow field through the volume of a sagging thin film.

Figure 9c-e displays three images of the plane located at the solid-liquid interface. Images were captured at various times throughout the experiment. The bright red dots represent the particles which appear to be stuck at the substrate boundary. Particle sedimentation occurs more prominently for the least viscous samples at lower incline angles (i.e., N35 at 5° incline). This leads to the observed velocity plateau previously discussed. Furthermore, particle sedimentation velocity was noted to be orders of magnitude smaller than the traverse velocity in the fallen liquid film. Thus, effects of particle sedimentation were not of concern.

4.4. Limitations of the Utilized Particle Tracking Technique. Figure 10 displays an operational diagram to outline the limitations imposed by the utilized video microscopy setup. The trapewidal area shaded in blue outlines the accessible operational region. This region represents operation boundaries for a ROI of 989 X 802 pixels with a particle size ~30 pixels. The x-axis represents the frames per second set during video capture. The maximum rate attainable with a camera in our laboratory is 15,000 FPS. This limit is represented by the vertical line. The *y-axis* is the range of velocity values that can be measured. The top and bottom diagonal lines represent the upper and lower velocity bounds, respectively. The upper bound was set by assuming infinite dilution in which roughly one particle appears in the region analyzed. The lower bound assumes maximum particle packing possible for spherical shaped particles as estimated by a two-

https://doi.org/10.1021/acs.langmuir.2c01232
Langmuir 2022, 38, 11581-11589

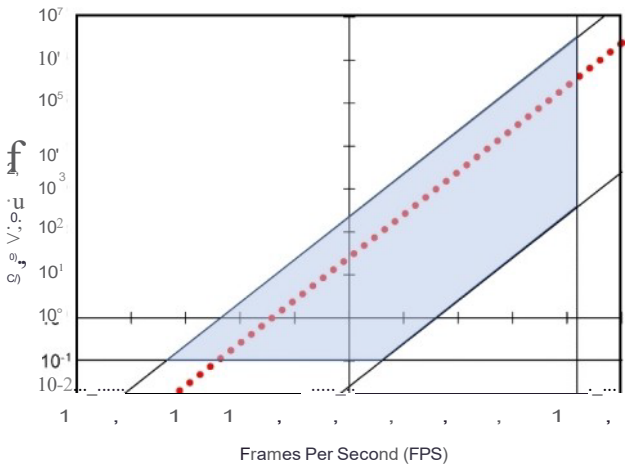

Figure 10. Operational diagram which displays the practical limitations for tracking sag with VAIM. The blue trapezoidal region represents the operational region accessible by the setup. The top and bottom diagonal lines represent the upper and lower bounds of velocity values that can be obtained. The upper bound assumes infinite dilution, whereas the lower bound assumes maximum packing. The red line is the operation line which assumes ~50 particles within the ROI. The horizontal black line represents static error in measurement obtained by measuring the velocity of particles which appear to be stationary at the interface. The vertical solid black line represents the maximum number of frames per second feasible with a camera in our laboratory.

dimensional hexagonal closed packed system. This value, which depends on the average ROI of ~793,178 pixels^2, was calculated to be ~ 1010 particles. The red line represents the operation line which corresponds to tracking SO particles in our ROI (roughly our work described herein). The horizontal line represents the static error associated with the measurement. This value was obtained by tracking the velocity of particles which appeared to be stuck at the solid liquid interface. Static error was measured to be ~0.1 $\mu m/s$. The setup used herein utilized IO FPS during video capture and predicted a maximum velocity of~ 100 $\mu m/s$. This prediction agrees with the maximum velocity measured as obtained via particle tracking at the film free surface.

The operational diagram pictorially displays an information-decision procedure, which can aid in the equipment selection process. Moreover, it can be used to help guide the use of the VAIM technique. The camera capabilities (i.e., frames per second) determine the maximum sag velocity that can be tracked with this instrument. For instance, IO FPS can capture a flow velocity of up to ~ 100 $\mu m/s$. Low viscosity materials will require adjusting (increasing) the FPS, such that the maximum particle velocity, which occurs at the free surface, is captured. Additionally, the measured velocity can be used to predict other parameters such as film thickness, particle tracking plane position relative to the substrate, orientation angle, or material viscosity. The interplay between the mentioned parameters is depicted in the expression displayed in eq 4. The VAIM operational diagram demonstrates a large experimental space to probe a variety of flowable materials with various substrate chemistries, testing temperatures, and UV curing apparatus incorporation.

5. CONCLUSIONS

Work presented herein concerns a new method for probing the kinematics of sagging thin films. Particle tracking measurements conducted through the volume of a thin film and at systematically varied gravitational stress were facilitated by a variable angle inspection microscope (VAIM). Three Newtonian films with known viscosities, ranging between 0.069 and 0.504 Pa s, were evaluated at both 5 and 10° incline angles. Our measurements were compared to a predictive model that incorporated the effects of gravity, in addition to a fitting parameter Gamma f', thought to be related to the downstream liquid film geometry. Our results showed film thinning to be a universal process with an expected relationship between viscosity, gravitational stress, and sag velocity. From our results, we conclude that the VAIM is an effective tool for measuring the sag flow field associated with a liquid film. We further conclude based on our operational diagram that the VAIM has a large experimental space to probe a variety of flowable materials with various substrate chemistries, testing temperatures, and curing techniques. This work introduces a new rheological tool capable of subjecting a liquid film to a specific gravitational stress. Future work will extend this unique method to flashing systems, which will experience more complex flow fields because of rapid solvent evaporation and transient changes in viscosity. This new technique shows promise for further developing the fundamental understanding of fluid flow on surfaces with various geometries and roughness. This thickness resolved method will enable the investigation of the synergetic effects of both fluid composition and substrate properties on the measured flow fields.

■ ASSOCIATED CONTENT

G Supporting Information

The Supporting Information is available free of charge at https://pubs.acs.org/doi/10.1021/acs.langmuir.2c01232.

SEM images of probe particles and additional analysis details and materials including photographs of the experimental setup (PDF)

■ AUTHOR INFORMATION

Corresponding Author

Marola W. Issa - *Department of Chemical and Biomolecular Engineering, Case School of Engineering, Case Western Reserve University, Cleveland, Ohio 44106, United States;* • orcid.org/0000-0002-8099-0459; Email: mwi8@) case.edu

Authors

Hairou Yu - *Department of Chemical and Biomolecular Engineering, Case School of Engineering, Case Western Reserve University, Cleveland, Ohio 44106, United States*

Maria Chiara Rollin - *Department of Chemical and Biomolecular Engineering, Lehigh University, Bethlehem, Pennsylvania 18015, United States*

Steven V. Barancyk - *PPG Industries, Inc., Pittsburgh, Pennsylvania 15272, United States*

Reza M. Rock - *PPG Industries, Inc., Pittsburgh, Pennsylvania 15272, United States*

James F. Gilchrist - *Department of Chemical and Biomolecular Engineering, Lehigh University, Bethlehem, Pennsylvania 18015, United States*

Christopher L. Wirth - *Department of Chemical and Biomolecular Engineering, Case School of Engineering, Case Western Reserve University, Cleveland, Ohio 44106, United States*

Complete contact information is available at: https://pubs.acs.org/10.1021/acs.langmuir.2c01232

Author Contributions

IIM.W.L and H.Y. contributed equally to this work.

Notes

The authors declare no competing financial interest.

■ ACKNOWLEDGMENTS

This work was supported by the National Science Foundation (NSF) award nos. 1931636 (C.L.W. and R.M.R.) and 1931681 Q.F.G.).

■ REFERENCES

(1) Eley, R.R.; Schwartz, L. W. Interaction of rheology, geometry, and process in coating flow. *J. Coating Technol.* 2002, 74-53. DOI: 10.1007/BF02697974.

(2) Lade, R. K; et al. Sag in dryingcoatings: Prediction and real time measurement with particle tracking. *Prog. Org.Coat.* **2015,** *86,* 49-58.

(3) Zaid, **A. N.** A Comprehensive Review on Pharmaceutical Film Coating: Past, Present, and Future. *Drug Des. Dev. Ther.* 2020, *Volume 14,* 4613.

(4) Lade, R. K; Musliner, A. D.; Macosko, C. W.; Francis, L. F. Evaluating sag resistance with a multinotched applicator: correlation with surface flow measurements and practical recommendations. *J. Coat. Technol. Res.* **2015,** *12,* 809.

(5) Croll, S. G.; Kisha, L. W. Observations of sagging in architectural paints. *Prog. Org. Coat.* 1992, 20, 27.

(6) Bornside, D. E.; Macosko, C. W.; Scriven, L. E. Spin coating: One-dimensional model. *J. Appl. Phys.* 1989, 66, 5185.

(7) Duskova-Smrckova, **M.;** Dusek, K Processes and states during polymer film formation by simultaneous crosslinking and solvent evaporation. *J. Mater. Sci.* 2002, *37,* 4733.

(8) Tushinsky, L. I.; Kovensky, I.; Plokhov, A.; Sindeyev, V.; Reshedko, P. *Mechanical Properties of Coatings;* Springer, 2002.

(9) Glass, J. E.; Prud'homme, R. K Coating Rheology: Component Influence on the Rheological Response and Performance of Water-Borne Coatings in Roll Applications. *Liquid Film Coating;* Springer Netherlands: Dordrecht, 1997.

(10) Feng, L.; Ulutan, D.; Mears, L. Energy consumption modeling and analyses in automotive manufacturing final assembly process. *2015 IEEE Conference on Technologies for Sustainability (SusTech);* IEEE, 2015.

(11) Bosma, M.; Brinkhuis, R.; Rensen, E.; Watson, R. A new method for the quantitative determination and prediction of sag and levelling in powder coatings. *Prog. Org. Coat.* 2011, 72, 26-33.

(12) Overdiep, W. S. The effect of a reduced solvent content of solvent-borne solution paints on film formation. *Prog. Org. Coat.* 1986, *14,* 1-21.

(13) Frisch, H. L.; Scopazzi, C. Sag equation for coatings on rotating substrates. *J. Appl. Polym. Sci.* 1991, *43,* 1067.

(14) Wu, S. Rheology of high solid coatings. II. Analysis of combined sagging and leveling. *J. Appl. Polym. Sci.* 1978, 22, 2783-2791.

(15) Lin, T. S.; Kondic, L.; Filippov, A. Thin films flowing down inverted substrates: Three-dimensional flow. *Phys. Fluids* 2012, *24,* 022105.

(16) Balmforth, N. J.; Craster, R. v.; Rust, A C.; Sassi, R. Viscoplastic flow over an inclined surface. *J. Non-Newtonian Fluid Mech.* 2006, *139,* 103.

(17) Kondic, L. Instabilities in gravity driven flow of thin fluid films. *SIAM Rev.* 2003, *45,* 95.

(18) Bonn, D.; Eggers, J.; Indekeu, J.; Meunier, J.; Rolley, E. Wetting and spreading. *Rev. Mod. Phys.* 2009, *Bl,* 739.

(19) Oron, A.; Davis, S. H.; Bankoff, S. G. Long-scale evolution of thin liquid films. *Rev. Mod. Phys.* 1997, 69, 931.

(20) Huppert, H. E. Flow and instability of a viscous current down a slope. *Nature* 1982, *300,* 427.

(21) Ruyer-Quil, C.; Trevelyan, S. P. M. J.; Giorgiutti-Dauphine, F.; Duprat, C.; Kalliadasis, S. Film flows down a fiber: Modeling and influence of streamwise viscous diffusion. *Eur. Phys. J.: Spec. Top.* 2009, *166,* 89.

(22) Espin, L.; Kumar, S. Sagging of Evaporating Droplets of Colloidal Suspensions on Inclined Substrates. *Langmuir* 2014, *30,* 11966-11974.

(23) Tiwari, N.; Davis, J. M. Stabilization of thin liquid films flowing over locally heated surfaces via substrate topography. *Phys. Fluids* 2010, 22, 042106.

(24) Schwartz, L. W.; Eley, R. R. Flow of architectural coatings on complex surfaces; Theory and experiment. *J. Eng. Math.* 2002, *43,* 153.

(25) Troian, S. M.; Herbolzheimer, J. F.; Safran, S. A.; Joanny, J. F. Fingering instabilities of driven spreading films. *Europhys. Lett.* 1989, *10,* 25.

(26) Thompson, P.A.; Troian, S. M. A general boundary condition for liquid flow at solid surfaces. *Nature* 1997, *389,* 360-362.

(27) Method, S. T. Standard Test Method for Sag Resistance of Paints Using a Multinotch Applicator 1. *Order a Journal on the Theory of Ordered Sets and Its Applications;* Springer, 1999; Vol. *06.*

(28) Hennessy, M. G.; Munch, A. Dynamics of a slowly evaporating solvent-polymer mixture with a deformable upper surface. *IMA J. Appl. Math.* 2014, *79,* 681. Institute of Mathematics and Its Applications)

(29) Wu, S. Rheology of high solid coatings. I. Analysis of sagging and slumping. *J. Appl. Polym. Sci.* 1978, 22, 2769.

(30) Schechter, R. S.; Byron, R.; Stewart, W. E.; Lightfoot, E. N. Transport Phenomena (Bird, R. Byron; Stewart, Warren E.; Lightfoot, Edwin N.). *J. Chem. Educ.* 1961, *38,* A640.

(31) LaPorte, R.J. *Hydrophilic Polymer Coatings for Medical Devices;* Routledge, 2017.

(32) Nong, K; Anderson, D. M. Thin film evolution over a thin porous layer: Modeling a tear film on a contact lens. *SIAM J. Appl. Math.* 2010, 70, 2771.

(33) Pease, L. F.; Russel, W. B. Electrostatically induced submicron patterning of thin perfect and leaky dielectric films: A generalized linear stability analysis. *J. Chem. Phys.* 2003, *11B,* 3790.

(34) Stober, W.; Fink, A.; Bohn, E. Controlled growth of monodisperse silica spheres in the micron size range. *J. Colloid Interface Sci.* **1** 68, 26, 62.

(35) Ekici, O.; Aslanta§, K; Karuk, O.; Kele§, A. Evaluation of surface roughness after root resection: An optical profilometer study. *Microsc. Res. Tech.* 2021, *84,* 828.

(36) Crocker, J. C.; Grier, D. G. Methods of digital video microscopy for colloidal studies. *J. Colloid Interface Sci.* 1996, *179,* 298.